JOURNAL OF SOLID STATE CHEMISTRY 111, 322–329 (1994)

An Anomaly in the Hydrogen-Bond System in Mixed Deuterated Magnesium–Iron Fluosilicates

G. Chevrier

Laboratoire Léon Brillouin (CEA-CNRS), C. E. N. Saclay, 91191 Gif-sur-Yvette Cedex, France

Received May 14, 1993; in revised form September 23, 1993; accepted October 4, 1993

Crystals $Mg_{1-\delta}Fe_\delta SiF_6 \cdot 6D_2O$ (δ = 0.11, 0.17, 0.50, and 1) have been studied using neutron diffraction (respectively: F_{000} = 43.32, 43.63, 42.09, 44.82; D_x = 1.86, 1.88, 1.94, 2.02 g · cm^{-3}; μ = 0.25, 0.24, 0.31, 0.23 cm^{-1} (evaluated); a = 9.571(8), 9.567(10), 9.587(8), 9.639(16) Å; c = 9.729(8), 9.717(12), 9.714(7), 9.690(15) Å; V = 772(2), 770(3), 773(2), 780(4) Å^3; space group P-3(147); trigonal, Z = 3). The final R-factors (0.087, 0.083, 0.070, and 0.044) were obtained using 382, 302, 270, and 170 observed structure factors. The structure remains the same in the four crystals, but a positional anomaly is found for the D(2) atom in the $Mg_{0.83}Fe_{0.17}SiF_6 \cdot 6D_2O$ compound. Details (temperature and hysteresis) on the known structural transitions of these compounds are presented. Furthermore, in the case of $FeSiF_6 \cdot 6D_2O$, a new transition is described.

INTRODUCTION

The fluosilicates $MSiF_6 \cdot 6H_2O$ are distributed into two series according to the structure of the high-temperature phase. In the first one (M = Co, Ni, and Zn), the structure is described in the R-3 space group: the two octahedral complex ions $M(H_2O)_6^{2+}$ and SiF_6^{2-} are placed in two orientations around the threefold axis (1–4). In the second one (M = Mg, Fe, and Mn), the presence of superstructure reflections, inconsistent with the model of Syoyama and Osaki (5) and Hamilton (6), leads to the use of the P-3 space group: the crystal presents two types of domains with different orientations of the complex ions, which are related by pseudomirrors (11.0) (1, 7–11). The presence and the exploitation of the superstructure reflections show that in the case of Mg and Mn compounds (1, 8, 9), the equal volume domains are large (typically 300 Å), whereas in Fe fluosilicate (1, 10) their size is a function of the temperature (typically 300 Å at 240 K and 96 Å at 300 K).

For the majority of these compounds, a structural phase transition is observed with decreasing temperature. The resulting structure is monoclinic $P2_1/c$, as determined by Syoyama and Osaki (5) for $MgSiF_6 \cdot 6H_2O$. The transition temperatures have already been reported in (1, 4, 5, 7–17).

After the neutron diffraction study of $MgSiF_6 \cdot 6D_2O$ (11), it seems of interest to us to undertake new diffraction analyses on mixed $Mg_{1-\delta}Fe_\delta SiF_6 \cdot 6D_2O$ in their high-temperature phase in order to determine precisely the evolution of the hydrogen bond system when the composition of iron is increased.

Furthermore, the phase transition in these mixed fluosilicates has been studied in detail.

EXPERIMENTAL

Large crystals of $Mg_{1-\delta}Fe_\delta SiF_6 \cdot 6D_2O$ (estimated degree of deuteration of about 70–80 at.%) were grown from a mixed saturated solution using the same technique as described elsewhere (4). The proportions of iron in the basic solution were 0.29 (crystal A), 0.50 (crystal B), 0.75 (crystal C), and 1.00 (pure $FeSiF_6 \cdot 6D_2O$, crystal D). From the first solution, transparent white prismatic crystals were obtained. With increasing iron composition, crystal colors turned to transparent green (crystal A, 3.8 × 2.5 × 1.5 mm; crystal B, 5 × 3 × 2 mm; crystal C, 5 × 3.5 × 2.5 mm; crystal D, 3.2 × 1.2 × 1.5 mm).

Bragg intensities were collected on the four-circle diffractometer P110 at the Orphée reactor (CEN Saclay, France) at a neutron wavelength of λ = 0.8307(5) Å. For crystals B and C, a decrease of the standard reflections (300) and (003) was observed (1.4% per hour and 1.5% per hour, respectively) and corrected. To avoid such an effect, crystals A and D were put under He gas in a sealed aluminum container: the intensities of the standard reflections (030) and (112) showed no variations within 2.1%. The other experimental parameters are given in Table 1.

The data were corrected for Lorentz effects, and since absorption is small (0.23 < calculated μ < 0.31 cm^{-1}), no corrections were applied. Only the structure factors with $F_0 > 3\sigma(F_0)$ were used for the structure refinements.

The neutron scattering lengths for Mg, Fe, Si, F, D, H, and O were taken as $b_{Mg} = 0.5375 \times 10^{-12}$, $b_{Fe} = 0.954 \times 10^{-12}$, $b_{Si} = 0.4149 \times 10^{-12}$, $b_F = 0.565 \times 10^{-12}$, $b_D = 0.6674 \times 10^{-12}$, $b_H = -0.3741 \times 10^{-12}$, and b_O =

0022-4596/94 $6.00

TABLE 1
Experimental Parameters and Refinement Results

	Crystal A	Crystal B	Crystal C	Crystal D
		Centering		
Number of reflections	16	18	17	21
Angle range	← 20.4°< 2θ < 51.8° →			
		Collection		
2θ range (°)	3–63 (unique set)	3–50	3–50	3–50 (unique set)
sinθ/λ (Å^{-1})	0.032/0.629		0.032/0.509	
Scan type	← ω-scan →			
Number of steps	← 41 →			
Scan time (sec)	1.8–4	2–6	2–6	2–6
Measured reflections	923	797	922	569
Unique reflections with $I_0 > 3\sigma(I_0)$	382	302	270	170
Temperature (K)	303	296	296	243
		Refinement		
$R(F)$	0.087	0.083	0.070	0.044
$R(F^2)$	0.102	0.082	0.050	0.050
Goodness of fit	4.26	5.83	5.31	2.06
Number of parameters	46	45	46	45

0.5805×10^{-12} cm (18). An isotropic extinction correction by the method of Zachariasen (19) led respectively to $G = 0.032(12)$, 0.099(14), 0.083(11), and 0.018(15) for the four crystals A, B, C, and D. The full matrix least-squares refinement method based on F^2 was used. The final R-factors, $R(F^2)$ and $R(F)$ ($(\Delta/\sigma)\max < 0.01$), the goodness of fit, and the number of refined parameters are given in Table 1. The computer program used in the refinements was XFLS (20) adapted to the treatment of antiphase domains, and the computers were a CONVEX C1-XP and a SUN 4-370.

On both sides of the phase transition, special reflections were followed with steps in temperature adapted to the variation of the intensity, using a closed-cycle refrigerator. The intensities were then computed from ω-step scans (41 steps, 2 to 6 sec per step) and the time between each two temperature changes was taken as 10 min.

THE TWO MODELS

$MgSiF_6,6D_2O$ Model

The structural model of $MgSiF_6 \cdot 6D_2O$ in its high-temperature phase has already been reported several times.

Figure 1a presents the projection onto the (00.1) plane of the cell corresponding to a domain, II, containing two "right" $Mg(D_2O)_6^{2+}$ octahedra and one "left" $Mg(D_2O)_6^{2+}$ octahedron, and two "left" SiF_6^{2-} octahedra and one "right" SiF_6^{2-} octahedron. Deviations of $Mg(D_2O)_6^{2+}$ and SiF_6^{2-} octahedra from the pseudomirror (11.0) are indicated; the atomic positions of Mg are 0 0 0, $\frac{2}{3}, \frac{1}{3}, \frac{1}{3}$, and $\frac{1}{3}\ \frac{2}{3}\ \frac{2}{3}$, and those of Si are 0 0 $\frac{1}{2}$, $\frac{2}{3}\ \frac{1}{3}\ \frac{5}{6}$, and $\frac{1}{3}\ \frac{2}{3}\ \frac{1}{6}$. The atomic positions of O, F, D(1), and D(2) are the 6*g* positions of the space group *P*-3: for O they are *xyz* . . . for a "right" orientation and $-y\ -x\ z$ . . . for a "left" one. For F, they are respectively $-y'\ -x'\ z'$ . . . and $x'y'z'$ . . . ; for D(1), respectively $x''y''z''$ . . . and $-y''\ -x''z''$ . . . ; and for D(2), respectively $x'''y'''z'''$ . . . and $-y'''\ -x'''z'''$ . . . . Besides such domains, others with the opposite situation (one "right" $Mg(D_2O)_6^{2+}$ octahedron and two "left" $Mg(D_2O)_6^{2+}$ octahedra, and one "left" SiF_6^{2-} octahedron and two "right" SiF_6^{2-} octahedra) are present in the crystal (domain I).

With the same expresions as before (8, 9, 11), the structure factor squared for the basic reflections ($-h + k + l = 3n$) is $F^2 = ((2 - m)F_{AB'} + (1 + m)F_{A'B})^2$, where m is the volumetric proportion of the ordered domain I, $F_{AB'}$ is the structure factor derived from the form factor of the "right" $M(D_2O)_6^{2+}$ octahedron and the form factor of the "left" SiF_6^{2-} one, and $F_{A'B}$ is the structure factor derived from the form factor of the "left" $M(D_2O)_6^{2+}$ octahedron and the form factor of the "right" SiF_6^{2-} one.

For the superlattice reflections ($-h + k + l = 3n \pm 1$), the squared structure factor is $F^2 = \alpha(F_{AB'} - F_{A'B})^2$, where α is the rate of coherence ($\alpha = \frac{3}{4}$) indicates a coherent superposition of the diffraction intensities and $\alpha = 1$ indicates an incoherent one (9, 11).

Because the superlattice reflections present the same width as the basic ones, in the real space, the two types

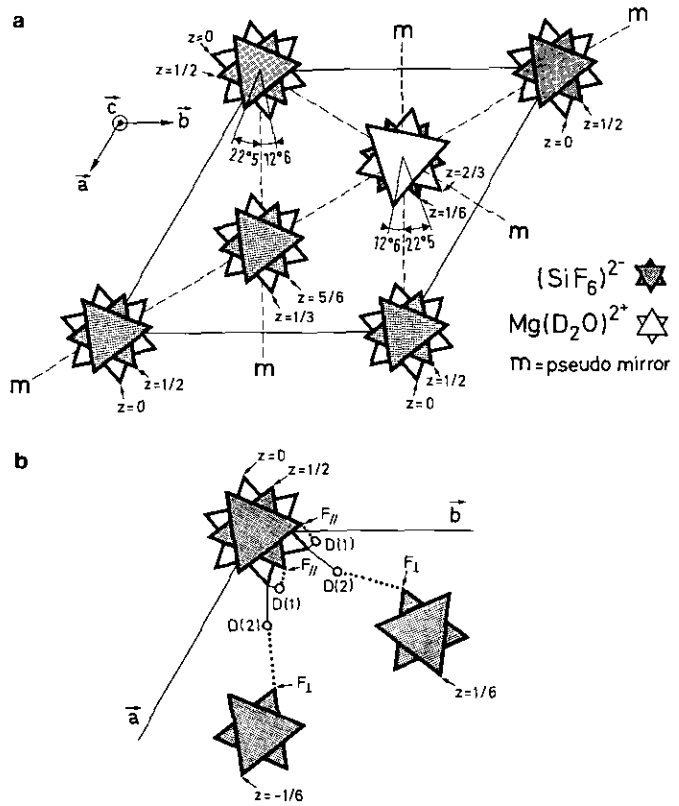

FIG. 1. Projection on the (00.1) plane of the cell corresponding to one type of domain in the case of $MgSiF_6 \cdot 6D_2O$ (11). (a) To simplify the drawing, the $Mg(D_2O)_6^{2+}$ octahedra ($z = 1$) which are projected on the SiF_6^{2-} octahedra ($z = 0.5$) are ommited, the Fe and Si atoms lie in the center of the corresponding octahedron, the values of the z parameter are the center of each octahedron, and the deuterium atoms are not included. (b) A detail of the packing shows the two hydrogen bonds $F_{//} \cdots D(1)$ and $F_\perp \cdots D(2)$ which are almost parallel and perpendicular to the three-fold axis.

of ordered domains (I) and (II) are large (typically 300 Å). The observed mirrors (11.0) are obtained when the value of m is near 0.5: the two types of domains contribute to the diffraction with an equal weight and the mirrors are then pseudomirrors.

$FeSiF_6,6D_2O$ Model

In the case of $FeSiF_6,6D_2O$, the superlattice reflections present a width which is a function of the temperature (typically 5.7° and 0.46° for the full width at half maximum (FWHM) of the 22.1 superlattice reflection at room temperature and 250 K, respectively, as compared to the 0.46° for the FWHM of the 13.1 basic reflection) and are observed out of the lattice points. In the real space, to explain the position and the width of the superlattice reflexions, one model was built where two types of domains (I) and (II) are present and whose extension is a function of temperature; in each type of domain (I) or (II), subdomains exist and the corresponding sublattices are connected by a translation of $\frac{2}{3}\,\frac{1}{3}\,\frac{1}{3}$. This previous model (10) leads to the expressions below.

For the basic reflections ($-h + k + l = 3n$) the squared structure factor is the same as before: $F^2 = ((2 - m)F_{AB'} + (1 + m)F_{A'B})^2$.

But, for the superlattice reflections ($-h + k + l = 3n \pm 1$), the presence of a translation leads to $F = \frac{1}{2}(F_{AB'} - F_{A'B}) + \frac{1}{4}(F_{AB'} - F_{A'B})(-1 + i * 3^{1/2})$ and $F^2 = \frac{1}{4}(F_{AB'} - F_{A'B})^2 = \beta(F_{AB'} - F_{A'B})^2$.

RESULTS AND DISCUSSION

Final atomic parameters and equivalent isotropic thermal parameters are given in Table 2. In the case of crystal B the first refinements of the atomic coordinates of D(2) led to $x = 0.1569(66)$, $y = 0.3057(11)$, and $z = 0.1065(9)$. However, constraining $y = 2x$ yields a significant reduction of the estimated standard deviation (ESD) (see Table 2) and of the number of the elements of the correlation matrix which exceeded 0.30 (from 37 to 13 elements). Consequently, in the P-3 space group, D(2) stays in the position 6*g*, although in the last cycles, x and y were constrained to $y = 2x$.

Refinements also lead to the real iron crystal composition, to the rate of deuteration, and to the values of the parameters m, α, or β (Table 3). The real iron crystal compositions as a function of the iron basic solution ones are drawn in Fig. 2. Respectively, they are 11(3), 17(4), and 50(3) at.%Fe in the crystals A, B, and C.

The results concerning the rates of deuteration for the four crystals confirm the values estimated from the prepa-

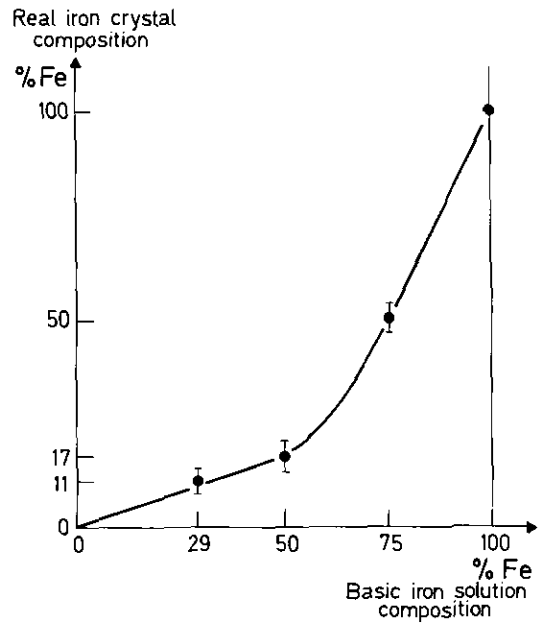

FIG. 2. Correspondence between the iron composition in the basic solution and in the crystal.

TABLE 2
Atomic Parameters and Isotropic Equivalent Temperature Factors

		Crystal B	Crystal B′		
	Crystal A	$y = 2x$	$y \neq 2x$	Crystal C	Crystal D
Mg					
x	0	0	0	0	
y	0	0	0	0	
z	0	0	0	0	
B_{eq} (Å^2)	1.70	1.60	1.62	1.75	
Fe					
x	0	0	0	0	0
y	0	0	0	0	0
z	0	0	0	0	0
B_{eq} (Å^2)	1.70	1.60	1.62	1.75	1.35
Si					
x	0	0	0	0	0
y	0	0	0	0	0
z	$\frac{1}{2}$	$\frac{1}{2}$	$\frac{1}{2}$	$\frac{1}{2}$	$\frac{1}{2}$
B_{eq} (Å^2)	1.51	1.54	1.52	1.68	1.51
F_L					
x	−0.1319(6)	−0.1324(6)	−0.1325(9)	−0.1338(5)	−0.1369(5)
y	−0.1530(6)	−0.1526(7)	−0.1526(9)	−0.1510(5)	−0.1486(6)
z	0.3999(5)	0.3999(6)	0.3999(7)	0.4001(6)	0.3999(5)
B_{eq} (Å^2)	2.60	2.65	2.65	2.75	2.16
O_R					
x	0.0613(7)	0.0623(8)	0.0629(14)	0.0673(7)	0.0821(15)
y	0.1968(6)	0.1974(7)	0.1973(11)	0.1995(6)	0.2030(5)
z	0.1245(5)	0.1242(6)	0.1242(9)	0.1254(6)	0.1265(4)
B_{eq} (Å^2)	3.15	3.24	3.26	3.50	3.67
$D(1)_R$					
x	0.0363(8)	0.0381(9)	0.0382(12)	0.0455(8)	0.0574(8)
y	0.1876(8)	0.1885(8)	0.1885(11)	0.1906(7)	0.1938(6)
z	0.2189(5)	0.2188(7)	0.2188(10)	0.2208(8)	0.2220(5)
B_{eq} (Å^2)	4.39	4.27	4.26	4.52	3.77
$D(2)_R$					
x	0.1376(20)	0.1530(3)	0.1569(66)	0.1356(12)	0.1480(23)
y	0.3044(6)	0.3060(3)	0.3057(11)	0.3068(6)	0.3104(5)
z	0.1065(5)	0.1067(6)	0.1065(9)	0.1060(7)	0.1039(5)
B_{eq} (Å^2)	4.14	4.71	4.75	3.95	4.67

Note. The atomic parameters of F_R, O_L, $D(1)_L$, and $D(2)_L$ are obtained from those of F_L, O_R, $D(1)_R$, and $D(2)_R$ with the transformation $-y$, $-x$, and z. B_{eq} is defined as $(8\pi^2/3) \cdot (u(3,3) + 4/3(u(1,1) + u(2,2)\text{-}u(1,2)))$. Crystal B is refined with a constraint on D(2) ($y = 2x$); crystal B′ is refined without constraint: the reduction of the ESD is clearly seen.

TABLE 3
Refined Values of the Rate of Deuteration and the m, α, and β Parameters

	Crystal A	Crystal B	Crystal C	Crystal D
Rate of deuteration	0.885(6)	0.891(6)	0.839(5)	0.895(5)
m parameters	0.497(7)	0.495(8)	0.495(7)	0.495(8)
α parameter	0.740(7)	0.743(7)	0.635(7)	—
β parameter	—	—	—	0.277(11)

ration of the compounds. The observed mirrors (11.0) are pseudomirrors, as the refined values of the m parameter is almost 0.5.

On the other hand, the rate of coherence α is obtained in the mixed crystals. In A and B, it seems that there is a complete disorder between Mg and Fe in the structure: the values of the α parameter stay near $\frac{3}{4}$ and the "magnesium model" is sufficient to explain all the observations. With increasing iron concentration, different areas of solid solution $Mg(Fe)SiF_6 \cdot 6D_2O$ and pure $FeSiF_6 \cdot 6D_2O$ can be created during the crystal growth; in the case of the crystal C the refined value of α is 0.635 instead of $\frac{3}{4}$. The volume proportion of the solid solution that is present in the crystal can be estimated to be $\eta = 0.77$, from the model values ($\alpha = \frac{3}{4}$ and $\beta = \frac{1}{4}$, and then $\eta * \alpha + (1 - \eta) * \beta = 0.635$). For this crystal, the width of the superlattice reflections is the same as that of a basic reflection, and furthermore none of them is observed out of the lattice points. As a consequence, the solid solution drives the averaged network, and the extension of the antiphase domains is always large. In the case of the crystal D (100% Fe), the value of the β coefficient is near the model value ($\beta = \frac{1}{4}$). This small discrepancy is certainly due to overestimation of the superstructure intensities induced either by possible disordered areas in the crystal or by the existence of antiphase boundaries which are not as regular as assumed in the model.

The analysis of the atomic positions (Table 2) and the bond distances and angles (Table 4) shows the following:

(i) The introduction of iron in the $MgSiF_6$, $6D_2O$ does not greatly modify the structure.

The Mg(Fe) atom is always octahedrally coordinated by water molecules with their planes almost within the threefold axis. The deviation stays near 10.5(9)° when passing from Mg to Fe compounds (respectively 11.1(8)° (11), 10.9(7)°, 9.5(8)°, 9.6(7)°, and 11.4(10)°).

With increasing iron composition, the substitution of Fe for Mg shows a tendency to symmetrize the $Mg(Fe)(D_2O)_6^{2+}$ octahedron: the difference in angles ((O–Mg(Fe)–O′)–(O–Mg(Fe)–O) varies from 2.2° (100% Mg, 11) to 1.2° (100% Fe, crystal D). The same tendency is observed in the case of the crystal D with the substitution of H by D: the difference (O–Fe–O′)–(O–Fe–O) is 1.2(5)° with 89.5% D, but it is around 3° with 100% H (10). The bond lengths Mg(Fe)–O stay almost the same (2.06 Å) with the weak iron concentrations (crystals A and B) and increase to 2.10 Å (crystal D). This last distance again shows the influence of deuterium: it is reduced from 2.143(8) Å (100% H, (10)) to 2.100(5) Å in the deuterated crystal.

Concerning the SiF_6^{2-} octahedra, the octahedron is very regular; its conformation remains between 0.4 and −0.4°. The bond lengths Si–F (averaged value 1.684(6) Å) are in agreement with the values found in the other fluosilicates (1.683(3) Å in Ni, 1.681(1) Å in Mn–fluosilicate).

The two types of octahedra ($Mg(Fe)(D_2O)_6^{2+}$ and SiF_6^{2-}) are connected by hydrogen bonds (Fig. 1b). To align the Mg–O and Si–F directions with the (11.0) pseu-

TABLE 4
Bond Distances (Å) and Angles (°) (Estimated Standard Deviations in Parentheses)

	Crystal A	Crystal B	Crystal C	Crystal D
Mg(Fe)–O	2.063(5)	2.062(6)	2.080(6)	2.100(5)
Si–F	1.685(5)	1.683(6)	1.681(5)	1.686(5)
O–D(1)	0.942(7)	0.941(9)	0.944(10)	0.949(7)
O–D(2)	0.934(8)	0.980(7)	0.922(7)	0.930(7)
O . . . $F_{\parallel}$	2.774(7)	2.774(9)	2.768(8)	2.769(8)
O . . . $F_{\perp}$	2.694(7)	2.692(9)	2.700(7)	2.728(8)
D(1) . . . $F_{\parallel}$	1.842(7)	1.843(9)	1.834(10)	1.831(8)
D(2) . . . $F_{\perp}$	1.823(8)	1.850(7)	1.821(7)	1.853(10)
O–Mg(Fe)–O	89.0(4)	89.2(4)	89.2(4)	89.4(5)
O–Mg(Fe)–O′[a]	91.0(4)	90.8(4)	90.8(4)	90.6(5)
Mg(Fe)–O–D(1)	123.0(9)	122.9(11)	122.6(11)	121.5(8)
Mg(Fe)–O–D(2)	127.3(10)	124.5(8)	128.9(10)	129.0(10)
F–Si–F	89.9(5)	89.9(5)	90.0(4)	90.2(5)
F–Si–F′[a]	90.1(5)	90.1(5)	90.0(4)	89.8(5)
O–D(1) . . . F	169.7(64)	169.6(80)	169.6(81)	169.6(66)
O–D(2) . . . F	154.1(28)	142.1(17)	158.8(31)	155.8(31)
D(1)–O–D(2)	107.9(13)	108.2(13)	107.7(14)	109.5(12)
γ1	12.3(3)	12.0(3)	10.6(3)	6.3(6)
γ2	22.7(4)	23.0(5)	24.0(3)	25.9(4)

[a] Along the z-axis, unprimed atoms lie on the up side of the octahedra (and primed ones on the down side).

domirror plane, it is necessary to turn them. The deviations, respectively $\gamma 1$ and $\gamma 2$, are a function of the iron composition of the crystal: while $\gamma 1$ shows a regular decrease from 12.6(2)° (11) to 6.3(6)° when passing from Mg to Fe compounds, $\gamma 2$ shows a linear increase from 22.5(4)° (11) to 25.9(4)°.

(ii) The O–D(1) distance presents a regular increase when the iron composition increases in the crystal, although the O–D(1) · · · F angle is always the same. By contrast, this regular increment is not presented by O–D(2) and D(2) · · · F distances, and the O–D(2) · · · F angle is not constant. An anomaly exists for the D(2) position in the case of the crystal B (Figs. 3a and 3b).

The first time, this observation was interpreted as an artefact of the refinement. However, a careful analysis allows us to refute this supposition. First, the regular increase of the O–D(1) distance and the coherent values of all the other bonds (Table 4) are factors which confirm the refinements; second, in the case of the

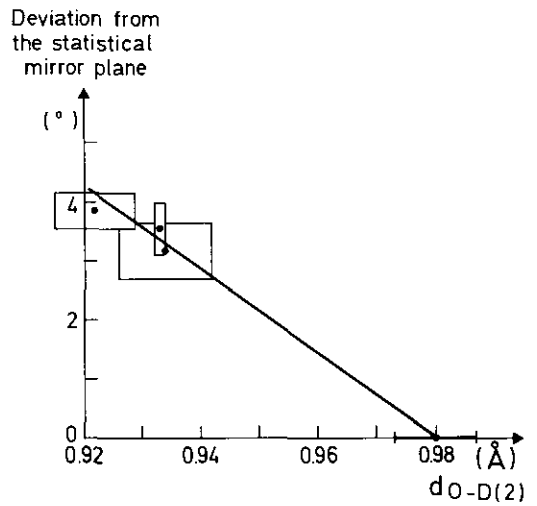

FIG. 4. Deviation of the D(2) atom from the pseudomirror plane (11.0), as a function of O–D(2) distance with estimated standard domains in $MgSiF_6 \cdot 6D_2O$ (11) and in the different crystals A, B, and C.

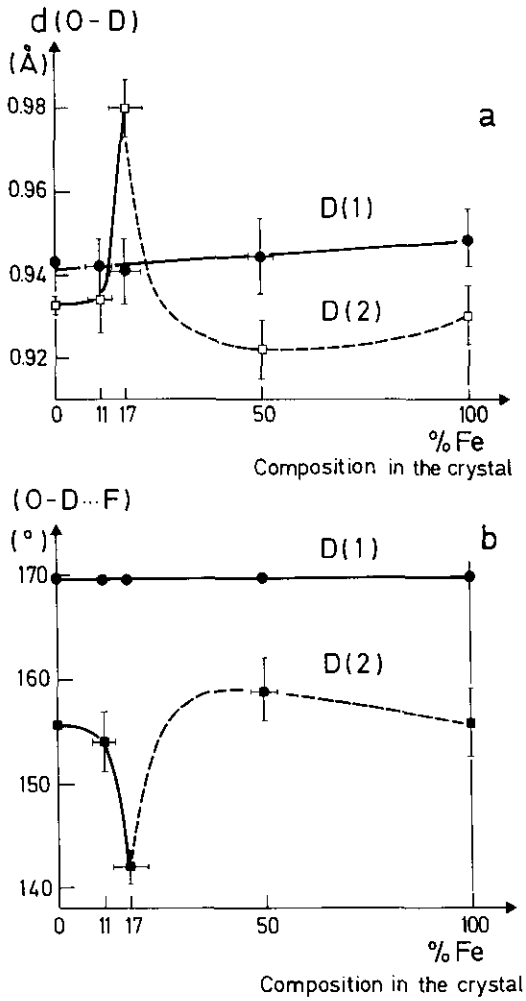

FIG. 3. Positional anomaly of the D(2) atom. O–D distance (a) and O–D · · · F angle (b) as functions of the iron composition in the crystal.

"$MgSiF_6 \cdot 6D_2O$ model" (crystals A, B, and C) and of the pure magnesium compound (11), it is noteworthy that the plotting of the deviation of the D(2) atom from the pseudomirror plane (11.0) as a function of the O–D(2) distance presents no divergence (Fig. 4). In fact, in crystal B, the D(2) atom is in the pseudomirror, which produces this position anomaly.

Furthermore, in this series, the averaged equivalent temperature factors of Mg, Si, O, D(1), and F are obtained with relatively poor standard deviations, respectively 1.69(7), 1.56(8), 3.28(16), 4.37(12), and 2.69(7) Å^2. This is also the case for D(2), 4.03(10) Å^2, when the corresponding value of crystal B is excluded (with it, the averaged B_{eq} is 4.20 Å^2, which is not very different, but with a far higher standard deviation, 0.35 Å^2). This anomaly is also seen in the ellipticity of the displacement ellipsoid, defined as "longest axis"/"shortest axis" (a/b) of the ellipsoid derived from the u_{ij}. The values of a/b for Mg, Si, O, F, D(1), and D(2) with the terms of crystal B excluded are respectively 1.03(1), 1.03(4), 1.82(6), 1.50(4), 1.72(3), and 1.58(12). But if the two parameters of D(2) of crystal B are included, the value of the displacement ellipsoid is 1.69(24), which is at the same time, higher for the averaged a/b and for the standard deviation. At this stage of discussion, the D(2) parameters (crystal B) B_{eq} = 4.71 Å^2 and b/a = 2.03 are to be compared with those obtained in the case of unconstrained refinement, B_{eq} = 4.75 Å^2 (almost the same value) and a/b = 2.36 (higher value). All these considerations show, without any uncertainty, that the substitution of iron for magnesium produces a compound where the D(2) atom lies in the pseudomirror, which leads to anomalies in its position and in its thermal parameters.

TRANSITION TEMPERATURE

As for $MgSiF_6 \cdot 6D_2O$, $MnSiF_6 \cdot 6D_2O$, and $CoSiF_6 \cdot 6D_2O$, the A, B, C, and D crystals show a first-order transition when the temperature is decreased (1, 5, 7, 8–17). This characterizes the change of the P-3 symmetry (high-temperature phase) to a $P2_1/c$ one (low-temperature phase), where a twinning is obtained with three orientations, each of them turned by 120°. Figures 5a and 5b show, as an example, the determination of the transition temperature and the range of the hysteresis in the C crystal: these two values are obtained from the variation of the intensity of a chosen diffraction peak as a function of the temperature. Figure 5c gives the transition temperature variation as a function of the iron composition: between pure $MgSiF_6 \cdot 6D_2O$ and pure $FeSiF_6 \cdot 6D_2O$, a very regular decrement of the temperature corresponding to the P-3 > $P2_1/c$ transition is observed.

In the high-temperature phase (P-3 space group), the case of the crystal D is different from that of the other crystals: another transition is seen with the study of the width of the superlattice reflections. The measure of the FWHM of these reflections between the phase transition (P-3 > $P2_1/c$: 233 K) and room temperature shows a peak broadening, which increases from 252 K, while the FWHM of the basic reflections remains constant. A hysteresis of 2 K (251.8–253.8 K, respectively, with a decreasing and an increasing temperature) is obtained (Fig. 6) This new transition characterizes the size of the antiphase domains: between 233 and 251.8 K, the antiphase domains

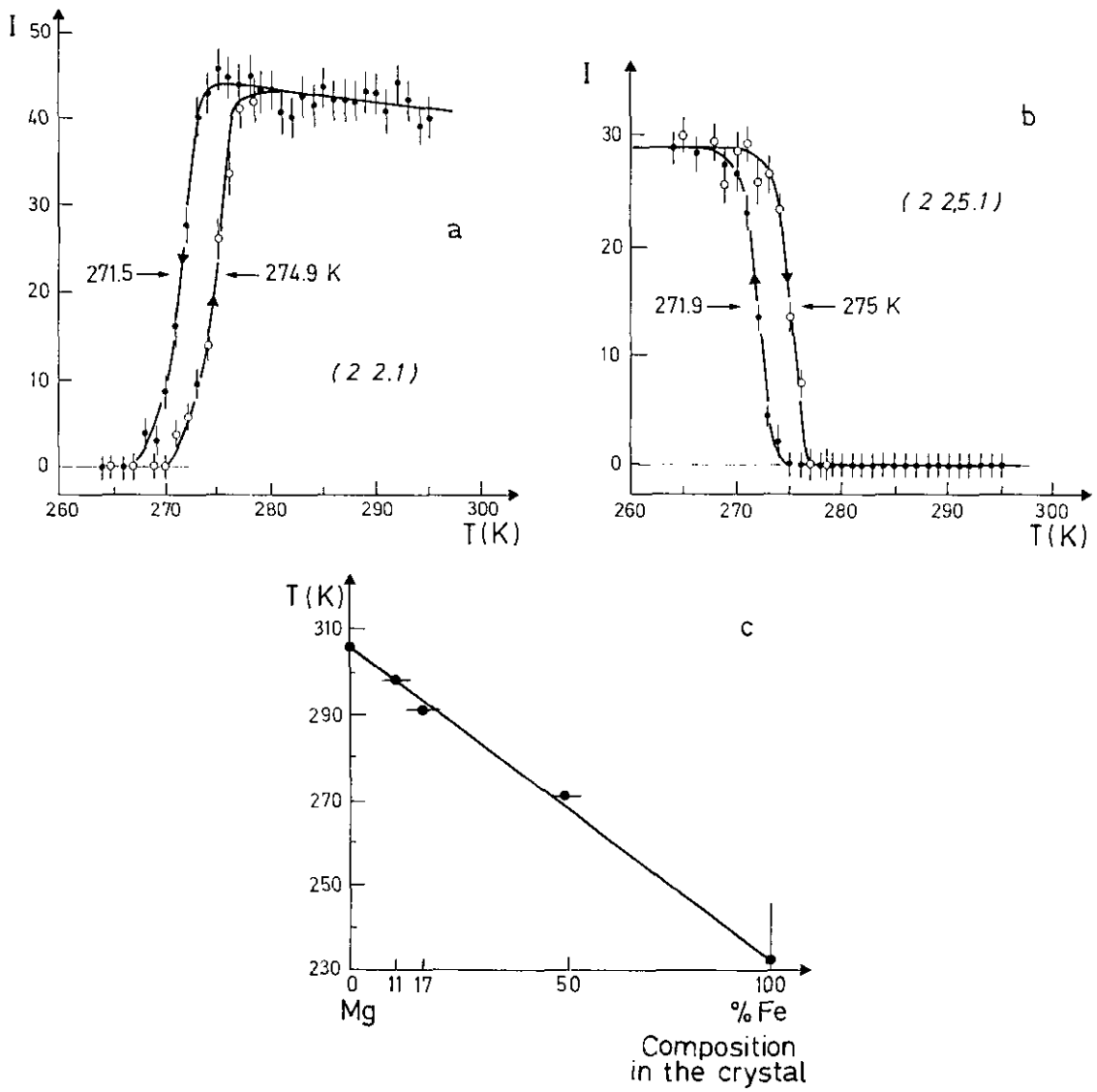

FIG. 5. (a,b) Intensity of (22.1) and (22, 5.1) peaks in the high-temperature phase of $Mg_{.50}Fe_{.50}SiF_6 \cdot 6D_2O$, as a function of temperature. (c) Transition temperature between the low-temperature ($P2_1/c$) and the high-temperature (P-3) phase, as a function of the iron composition in the crystal.

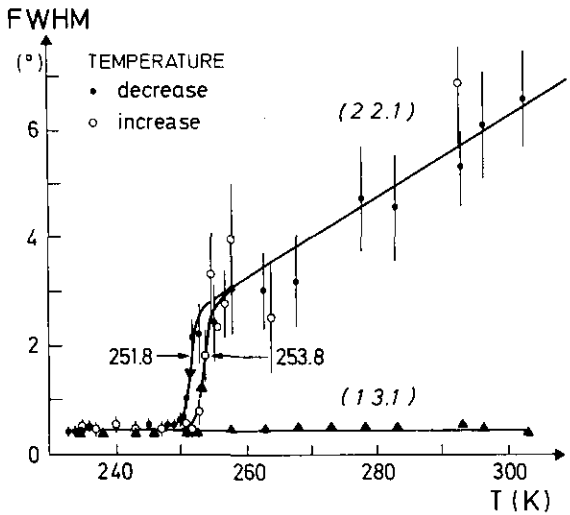

FIG. 6. Variation of FWHM of a basic reflection (13.1) and of a superlattice one (22.1) with the temperature.

stay very large (>250 Å), and their size decreases (96 Å at 300 K) above 251.8 K (1). It has to be investigated whether this could be related to the behavior of the octahedron rotation, which might be free above 251 K and frozen below.

CONCLUSION

This study shows that the previous model established for $MgSiF_6 \cdot 6D_2O$ can be used in mixed Mg–Fe fluosilicates up to 50% iron to explain the observed intensities. Only an anomaly in the hydrogen-bond system is displayed: the D(2) atom stays in the pseudomirror (11.0) when 17% iron are present in the crystal.

Studies on other mixed crystals ($x = 0.25$, $x = 0.70$, and $x = 0.90$) are now planned in order, first, to specify from which composition of iron the $FeSiF_6 \cdot 6D_2O$ model can be used and, second, to determine the composition of the domain where the D(2) anomalies occur.

ACKNOWLEDGMENTS

I am very grateful to H. Raynaud and A. Pinatel (DSM/DRECAM/SPEC CEN Saclay) for the preparation of the crystals.

REFERENCES

1. G. Chevrier, Thesis, University of Paris-Sud, Orsay, France, 1981.
2. D. C. Price, *Can. J. Phys.* **65,** 1280 (1987).
3. S. Ray, A. Zalkin, and D. Templeton, *Acta Crystallogr., Sect. B* **29,** 2741 (1973).
4. G. Chevrier and R. Saint-James, *Acta Crystallogr., Sect. C* **46,** 186 (1990).
5. S. Syoyama and K. Osaki, *Acta Crystallogr., Sect. B* **28,** 2626 (1972).
6. W. C. Hamilton, *Acta Crystallogr.* **15,** 353 (1962).
7. G. Jehanno and F. Varret, *Acta Crystallogr., Sect. A* **31,** 857 (1975).
8. G. Chevrier and G. Jehanno, *Acta Crystallogr., Sect. A* **35,** 912 (1979).
9. G. Chevrier, *Acta Crystallogr., Sect. B* **47,** 224 (1991).
10. G.Chevrier, A. Hardy, and G. Jehanno, *Acta Crystallogr., Sect. A* **37,** 578 (1981).
11. G. Chevrier, *J. Solid State Chem.* **99,** 276 (1992).
12. M. Majundar and S. K. Dutta, *J. Chem. Phys.* **42,** 418 (1965).
13. M. Das and A. K. Pal, *J. Phys. Chem. Solids* **48**(10), 903 (1955).
14. I. Tsujikawa and L. Couture, *J. Phys. Radium* **16,** 430 (1974).
15. S. M. Skjaeveland and I. Svare, *Phys. Scr.* **10,** 273 (1974).
16. R. D. Weir, K. E. Halstead, and L. A.K. Staveley, *J. Chem. Soc., Faraday Trans. 2* **81,** 189 (1985).
17. B. Ghosh, N. Chatterjee, A. N. Das, S. K. Dutta Roy, and A. Pal, *J. Phys. C* **10,** L527 (1977).
18. A. Delapalme, Internal Report DPhG.SDN/85/59, LLB-CEN-Saclay, France, 1985.
19. W. H. Zachariasen, *Acta Crystallogr.* **23,** 558 (1967).
20. W. R. Busing, K. O. Martin, and A. Lavy, "XFLS." Oak Ridge National Laboratory, Tennessee, 1977.